https://doi.org/10.33472/AFJBS.6.6.2024.5311-5327

African Journal of Biological Sciences

Journal homepage: http://www.afjbs.com

Research Paper Open Access

Development and characterization of Polymeric Nanoparticles for Optimizing Luliconazole Delivery in Tinea Versicolor Management

Prashil Suresh Dhumale[1], Shyamkumar Motiramji Dabhade[2], Dipali Subhash Doifode[3], Sonali Arun Kantale[4], Akshay Mukundrao Akotkar[5], Shubham Bajirao Ahir[6], Anuja Madhukar Rekhate[7], Ab Ahesan Ab Faruk[8*]

[1,5,8]Department of Pharmaceutics, Vidyaniketan College of Pharmacy Anjangaon surji District Amravati Maharashtra 444705.
[2,3,4]Department of Pharmaceutical Chemistry, Vidyaniketan College of Pharmacy Anjangaon surji District Amravati Maharashtra 444705.
[6]Department of Pharmaceutics, Dr Rajendra Gode College of Pharmacy Malkapur dist buldhana Maharashtra 443101.
[7]Department of Pharmacognosy and Phytochemistry, Vidyaniketan College of Pharmacy Anjangaon surji District Amravati Maharashtra 444705.

Corresponding Author: Ab Ahesan Ab Faruk[8*]
Department of Pharmaceutics, Vidyaniketan College of Pharmacy Anjangaon surji District Amravati Maharashtra 444705.

Article Info

Volume 6, Issue 6, June 2024

Received: 17 April 2024

Accepted: 20 May 2024

Published: 11 June 2024

doi: 10.33472/AFJBS.6.6.2024.5311-5327

ABSTRACT:

The research established the need to enhance drug delivery, while the current understanding and areas where information is lacking in this sector. The precise aims of the research, providing guidance for later investigations. By utilizing UV, FTIR, dissolution, zeta sizer and potential, SEM, and optical microscopy techniques, the study has effectively developed and assessed polymeric nanoparticles as a viable alternative. The process of creating batches showcased the real-world implementation of research discoveries, resulting in the production of enhanced polymeric nanoparticles. The results and discussions chapter analysed the findings from the characterization and evaluation experiments, offering insights into the possible effectiveness of the produced nanoparticles in managing tinea versicolor. This thorough investigation contributes to the progress of dermatological therapeutics, providing a hopeful pathway for enhanced treatment results in those suffering from tinea versicolor.

Keywords: Tinea versicolor, Fungal Infection, Skin Disease, Nanoparticles

1. INTRODUCTION

Tinea versicolor, a superficial fungal infection caused by the Malassezia genus, is characterized by the appearance of hypopigmented or hyperpigmented patches on the skin, typically on the trunk, neck, and upper arms [1]. While not considered medically serious, it can cause considerable distress due to its cosmetic effects. The challenges in treating tinea versicolor lie in its tendency for recurrence and the emergence of antifungal resistance. Current treatment modalities mainly include topical antifungal agents like ketoconazole, selenium sulfide, or oral medications such as fluconazole [2]. However, these treatments often necessitate prolonged use, leading to issues of patient compliance and potential side effects such as skin irritation or systemic toxicity. Addressing these challenges, researchers are exploring innovative approaches, including the utilization of polymeric nanoparticles in treatment strategies. Polymeric nanoparticles offer several advantages, including improved drug solubility, enhanced stability, and controlled release kinetics [3]. By encapsulating antifungal agents within biocompatible polymer matrices, nanoparticles can facilitate targeted delivery to the affected skin areas, thereby enhancing drug penetration and bioavailability while minimizing systemic exposure and adverse effects. Moreover, the sustained release provided by polymeric nanoparticles could potentially prolong the therapeutic effect, addressing the issue of recurrence in tinea versicolor treatment [4]. This approach holds promise for optimizing treatment efficacy and patient outcomes while minimizing the burden of prolonged therapy and associated side effects. Further research into the formulation, characterization, and clinical application of polymeric nanoparticles in tinea versicolor treatment is warranted to realize their full potential in clinical practice. Tinea versicolor, a common fungal infection of the skin, is primarily caused by members of the Malassezia genus, particularly Malassezia furfur. These lipophilic yeast-like fungi are part of the normal skin flora and usually inhabit the sebaceous glands and hair follicles. However, under certain conditions, such as warm and humid environments or alterations in the skin's lipid composition, Malassezia yeasts can proliferate excessively, leading to the development of tinea versicolor [5]. The pathogenesis of this condition involves several factors, including the production of lipases and other enzymes by Malassezia, which facilitate its adherence to and invasion of the stratum corneum, the outermost layer of the skin. Once established on the skin surface, Malassezia yeasts disrupt normal skin pigmentation by producing azelaic acid, a substance that inhibits the synthesis of melanin, resulting in the characteristic hypo- or hyperpigmented patches seen in tinea versicolor. Additionally, Malassezia-induced inflammation and immune responses contribute to the clinical manifestations of the infection. While the exact mechanisms underlying the transition of Malassezia from a commensal organism to a pathogen in tinea versicolor are not fully understood, factors such as genetic predisposition, hormonal fluctuations, immunosuppression, and excessive sweating are believed to play a role in predisposing individuals to this condition [6]. Overall, the etiology and pathogenesis of tinea versicolor involve a complex interplay between host factors, environmental conditions, and the virulence attributes of Malassezia yeasts, highlighting the multifactorial nature of this common dermatological disorder.

Tinea versicolor presents with distinctive clinical features characterized by the appearance of hypopigmented or hyperpigmented patches on the skin, typically on areas with a high density of sebaceous glands such as the trunk, neck, and upper arms. These patches may vary in size and shape, ranging from small, round lesions to larger, irregularly shaped areas [7]. The affected skin often has a fine, powdery scale, giving it a slightly scaly or velvety texture. In some cases, tinea versicolor lesions may be pruritic (itchy), particularly when sweating exacerbates the condition. The color of the patches can vary depending on individual skin

tone, with lighter-skinned individuals often developing darker patches and darker-skinned individuals exhibiting lighter patches [8]. Furthermore, tinea versicolor is known for its characteristic "maculae ceruleae" phenomenon, where affected areas may fluoresce yellow-green under Wood's lamp examination due to the fluorescent metabolites produced by Malassezia yeasts [9]. While tinea versicolor lesions are typically asymptomatic or mildly symptomatic, the cosmetic concerns associated with the condition can cause significant distress to affected individuals, impacting their quality of life. In addition to the typical presentation described, tinea versicolor may exhibit variations in its clinical appearance depending on factors such as skin type, duration of the infection, and the individual's immune response [10]. Some individuals may present with more extensive involvement, with lesions spreading to cover large areas of the trunk, neck, and extremities. Conversely, others may have localized or scattered patches with minimal involvement. Furthermore, tinea versicolor can sometimes mimic other skin conditions such as pityriasis rosea, vitiligo, or even early-stage psoriasis, emphasizing the importance of accurate diagnosis through clinical examination and, if necessary, laboratory tests such as skin scrapings for microscopy and culture [11]. While tinea versicolor is typically a chronic and relapsing condition, its clinical course may be influenced by various factors including seasonal changes, hormonal fluctuations (e.g., during puberty or pregnancy), and immunosuppression. Understanding the diverse clinical presentations of tinea versicolor is essential for clinicians to differentiate it from other dermatological conditions and to tailor appropriate management strategies, which may include topical or systemic antifungal therapy, maintenance therapy to prevent recurrence, and measures to address cosmetic concerns. Luliconazole has emerged as a promising treatment option for tinea versicolor, offering several advantages over traditional therapies. As a potent azole antifungal agent, luliconazole exerts its therapeutic effect by inhibiting the synthesis of ergosterol, a key component of fungal cell membranes [12]. This mechanism of action not only suppresses the growth of Malassezia yeasts responsible for tinea versicolor but also disrupts their cell membranes, leading to fungal cell death. Luliconazole is available in topical formulations, such as creams and lotions, allowing for direct application to affected skin areas [13]. Its excellent skin penetration and prolonged retention in the stratum corneum contribute to its efficacy in eradicating fungal infections. Moreover, luliconazole demonstrates a favorable safety profile with minimal systemic absorption and a low risk of adverse effects, making it suitable for both acute treatment and long-term maintenance therapy [14]. The convenience, efficacy, and tolerability of luliconazole make it an attractive option for patients and clinicians seeking effective management of tinea versicolor, providing a valuable addition to the therapeutic arsenal for this common dermatological condition [15].

2. MATERIALS:

This study aimed to use chitosan as a polymeric carrier for the drug Luliconazole, and improve its stability, solubility, and bioavailability using commonly used excipients such as mannitol and lactose in nanoparticle formulation. The organic solvents dimethyl sulfoxide and ethanol were used, along with cholesterol and PEG 2000. The equipment used in the study included a probe sonicator and a magnetic stirrer[16].

Preparation of Polymeric Nanoparticles by Solvent Evaporation Method:
Measure the required amounts of polyethylene glycol, soya lecithin, cholesterol, and dimethyl sulfoxide. Mix polyethylene glycol, soya lecithin, and cholesterol in ethanol. This mixture will serve as the organic phase. Dissolve Luliconazole (the drug) in DMSO and then dilute it in distilled water. This will be the aqueous phase. Slowly add the organic phase (containing

the dissolved lipids) drop by drop into the aqueous phase (containing the drug). Use a high-speed homogenizer or sonicator to create an emulsion. Place the emulsion in a rotary evaporator. Evaporate the organic solvent (DMSO and ethanol) under reduced pressure, leaving behind the drug-loaded polymeric nanoparticles. Centrifuge the solution to separate the nanoparticles. Wash the nanoparticles with distilled water to remove any residual solvent. Centrifuge the solution to separate the nanoparticles. Wash the nanoparticles with distilled water to remove any residual solvent [17].

Table 1: Composition of Polymeric nanoparticles of Drug and Excipients.

Batch	**Soya lecithin (mg)**	**Cholesterol (mg)**	**Solvents**		**PEG**	**Amount of Drug (mg)**
			Methanol (ml)	Ethanol (ml)		
F1	10	5	10	5	-	10
F2	50	5	10	5	-	10
F3	100	5	10	5	5	10
F4	10	5	10	5	-	10
F5	50	5	10	5	5	10
F6	100	5	10	5	5	10
F7	25	10	10	5	10	10
F8	75	5	10	5	-	10
F9	75	5	10	5	10	10
F10	25	10	10	5	-	10

Evaluation of formulated batches:

Percentage yield and entrapment efficiency of formulation batches

Yield percentage and entrapment efficiency are crucial evaluation criteria for formulation quantities. The percentage yield reflects the efficiency of the formulation process as a whole by comparing the actual quantity of the desired product obtained to its theoretical yield. A process that produces a high percentage yield is more efficient and cost-effective.

Yield Percentage = *(Weight of PEG-Nanoparticles/Total expected weight of extract and excipients) × 100*

Entrapment efficacy, on the other hand, quantifies the formulation's capacity to effectively encapsulate and retain the target substance. It is especially applicable in the development of drug delivery systems, where the objective is to obtain maximum drug entrapment within the carrier system. A high entrapment efficiency guarantees that a greater proportion of the active ingredient is effectively conveyed to the target site, thereby enhancing therapeutic efficacy and minimizing waste.

Entrapment efficiency (%) = *(Calculated drug content/Theoretical drug content) × 100*

In-vitro release of formulation

The in-vitro release of all the batches of nano suspension was conducted using the dialysis bag technique. A clean dialysis bag was soaked in distilled water and a measured quantity of the polymeric nanoparticles suspension was placed inside the dialysis bag, which was then sealed with thread. The sealed dialysis bag was placed in a dissolution apparatus filled with 900 ml of PBS pH 7.4, and the temperature was stabilized at 37°C ± 0.5°C with the help of the dissolution apparatus set to 100 rpm. Samples were taken at various time intervals, and throughout the procedure, the sink condition was maintained by replacing the withdrawn sample with fresh PBS. The drug content was determined by diluting the samples and using a UV-visible spectrophotometer at 296 nm. The formulation with the highest EE% and drug release was selected for further studies [18].

FTIR of Formulation batches & excipients.

The FTIR (Fourier Transform Infrared Spectroscopy) results play a pivotal role in the analysis and characterization of formulation batches. FTIR spectroscopy is a powerful analytical technique that provides valuable information about the chemical composition and structural properties of the samples. By measuring the absorption and interaction of infrared radiation with the molecules in the formulation, FTIR spectra offer insights into the functional groups, molecular bonds, and overall chemical fingerprint of the samples.

The FTIR results allows to identify and confirm the presence of specific functional groups and chemical bonds in the formulation. This information is crucial for assessing the chemical integrity and stability of the product. Additionally, FTIR analysis can detect any potential chemical interactions or transformations that may occur during the formulation process, including degradation, impurities, or changes in molecular structure. The FTIR of optimized batches of PEGylated nanoparticles with their interpretation is shown below in result section [19].

3. RESULTS AND DISCUSSION

Evaluation of formulation:

Percentage yield and entrapment efficiency of formulation batches

The entrapment efficiency of nanoparticles was ascertained by the centrifugal-ultrafiltration method. Practically, the supernatant obtained after centrifuging nanoparticles was analysed for the amount of unentrapped nanoparticles using spectrophotometer absorption in 296 nm wavelength, respectively [20]. As an aliquot (2 ml) of the drug-entrapped complexes was placed in the upper chamber of a centrifuge tube matched with a centrifugal-ultrafiltration tube. Then, the concentration of samples was calculated according to standard curves. All experiments were carried out at 25^{o} C. The entrapment efficiency and loading capacity were computed by the below equation:

Drug loading (%) *= Amount of drugs loaded in complex/Total weight of complex × 100.*

Entrapment efficiency (%) *= Weight of drugs added – Free drugs in supernatants/Weight of drugs added × 100.*

Table 2: Percentage yield and encapsulation efficiency of the batches

Formulation Batches	Percentage Yield (%)	Entrapment efficiency (%)
F1	56.84	55.24
F2	60.23	65.14
F3	77.12	78.86
F4	54.45	60.41
F5	54.78	62.54
F6	81.4	86.7
F7	66.3	72.5
F8	79.98	80.19
F9	77.6	82.9
F10	83.2	84.01

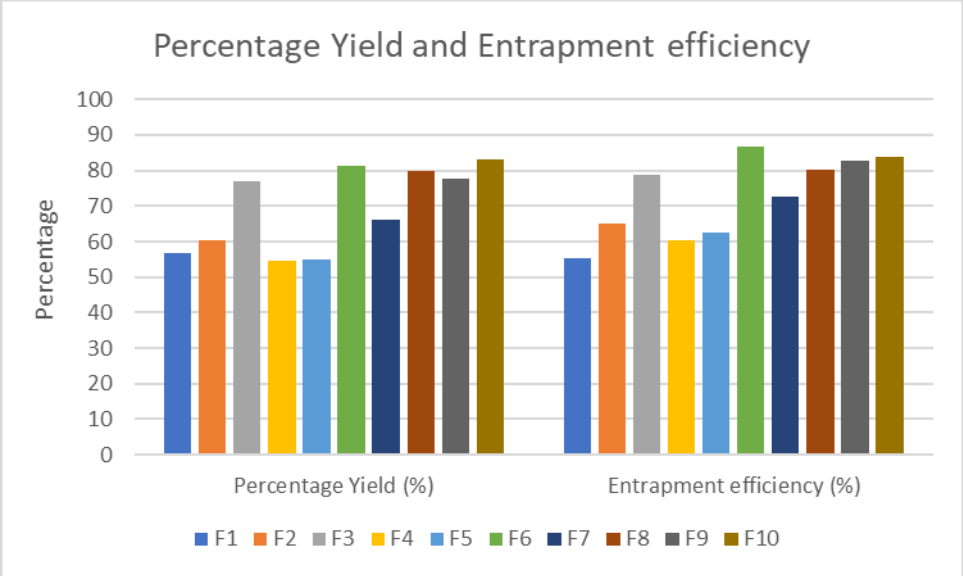

Figure 1: Column representation of percentage yield & entrapment efficiency of batch F1-F6.

In- vitro drug release study:

The in vitro drug release of formulations was investigated using a dialysis tube method. As drug release profile of formulation was evaluated in PBS, as pseudo physiological release medium, at pH = 7.4 and 37 ◦C. Practically, 2 ml of drug-entrapped nanoparticles was filled into a dialysis tube and the end sealed dialysis tube was immersed fully in 900 ml of the release medium in a dissolution flask with continuous stirring 50 rpm and 37 ◦C. Thereafter, 5 ml of the sample was withdrawn at different time intervals up to 2 hours and replaced with the same volume of fresh PBS (pH 7.4), and the amount of extract was quantified. The collected samples were analysed by shimadzu 1800 UV–vis Spectrophotometer at 296 nm wavelengths under the same analytic conditions [21].

Table 3 Percentage drug release profile of formulation batches.

Time point (hours)	**F1**	**F2**	**F3**	**F4**	**F5**	**F6**	**F7**	**F8**	**F9**	**F10**
0	0	0	0	0	0	0	0	0	0	0
1	12%	17%	16%	14%	11%	15%	13%	16%	10%	11%
2	27%	31%	33%	23%	24%	28%	22%	23%	26%	24%
3	48%	44%	51%	39%	38%	49%	46%	52%	47%	43%
4	61%	62%	66%	57%	55%	67%	61%	66%	59%	60%
5	79%	77%	82%	72%	73%	83%	78%	84%	72%	77%
6	92%	94%	96%	88%	87%	98%	90%	93%	88%	96%

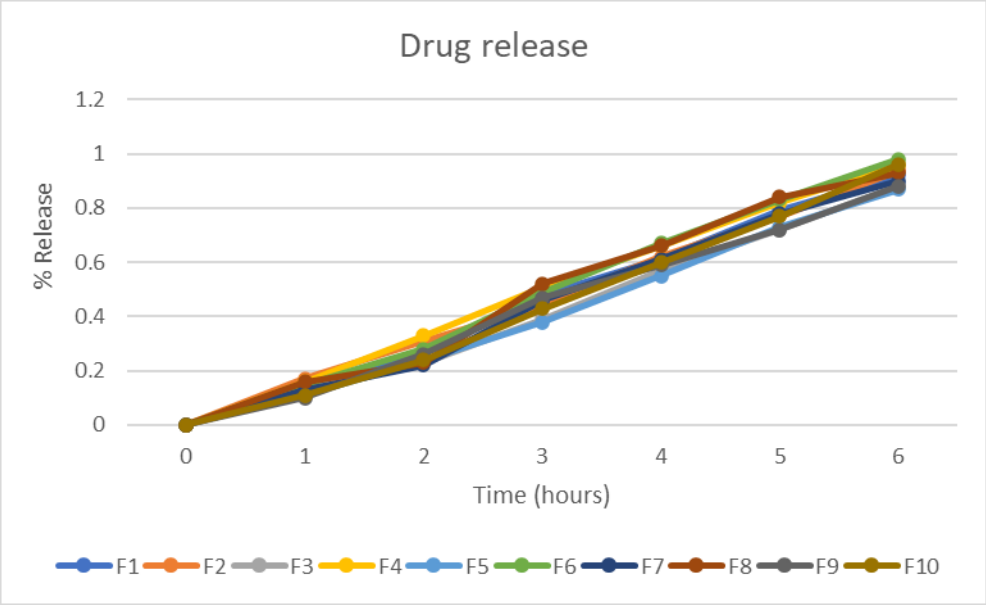

Figure 2: Cummulative drug release percentage (%).

FTIR analysis of excipients and formulation batches

FT-IR, as the other absorbance-based analytical technique was used to the characterization of synthesis quality by identifying organic and polymeric compounds. In FT-IR analyses, surface-modified and drug entrapped nanoparticles samples were analysed and results were processed using the software FT-IR spectrum [81].

FTIR study of drug used.

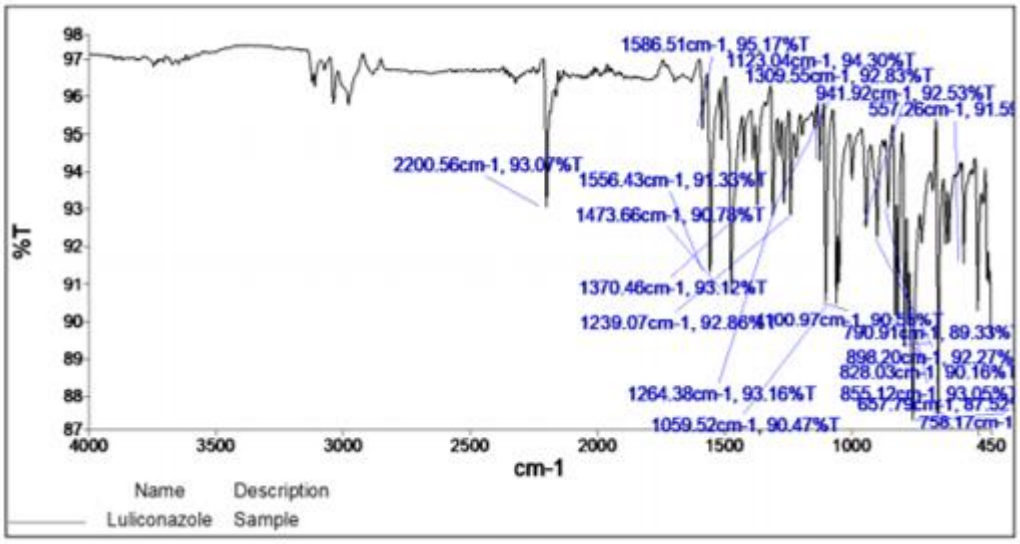

Figure 3 IR of Luliconazole

Table 4 IR interpretation of Luliconazole

Peak Range	Group	Class	Frequencies Determined
500–600	C─X	Bromoalkanes	501.49, 555.50
600-790	C─X	Chloroalkanes	624.94, 655.80, 763.8, 786.96
800–860	C─H	Para-disub. benzene	825.53, 856.39
900	C─H	Monosubstituted alkenes	902.69
990	C─H	Monosubstituted alkenes	995.27

~1100	C—O	Secondary alcohols	1103.28, 1643.22
1150–1200	C—O	Tertiary alcohols	1103.28, 1643.22
1220-1300	C—O	Carboxylic acids	1234.34, 1265.30, 1303.88, 1365.60
1450-1680	C═C	Aromatic C═C and conjugated C═C	1512.19, 1550.77, 1581.63, 1627.92
1710-1810	C=O	Carboxylic Acid	1735.93, 1774.51, 1813.09, 1859.38
1900	C=C=C	Alkene stretching bond	1890.24, 1936.53

FTIR study of excipients used.

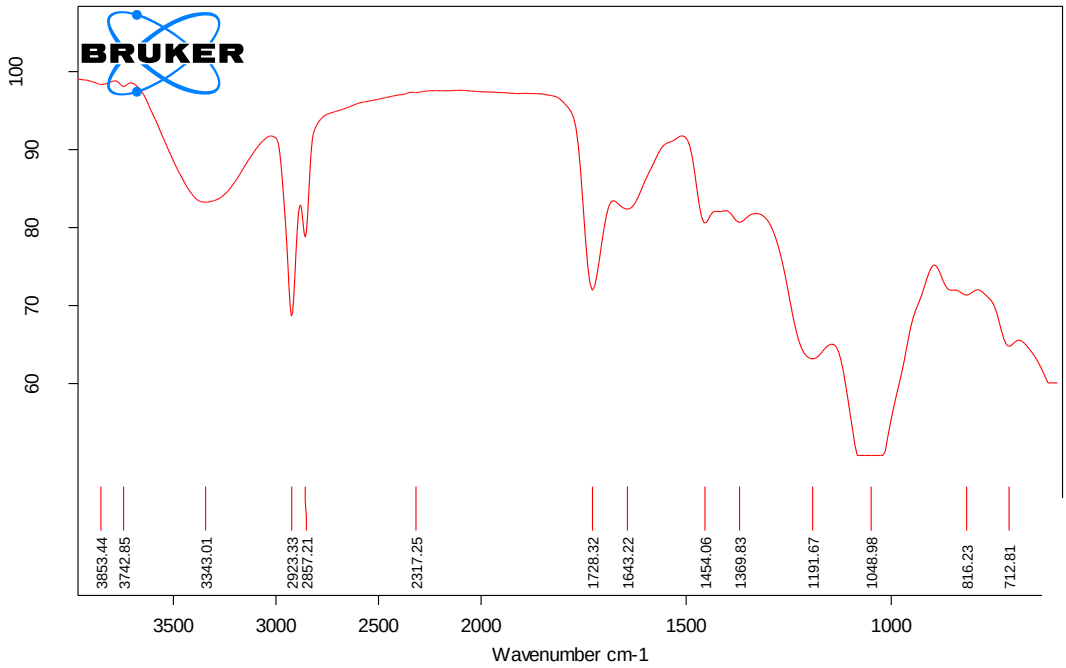

Figure 4 IR of soya lecithin

Table 5 IR interpretation of soya lecithin

Peak Range	**Group**	**Class**	**Frequencies Determined**
790-840	C=C bending	Alkene	816.23
1040-1050	CO-O-CO stretching	anhydride	1048.98
1163-1210	C-C stretching	Ester	1191.67
1335-1372	S=O stretching	sulfonate	1369.83
1450-1465	C-H bending	Alkane	1454.06
1640-1690	C=N stretching	imine/oxime	1643.22
1720-1740	C=O stretching	Aldehyde	1728.32
2840-3000	C-H stretching	Alkane	2857.21
2800-3000	N-H stretching	amine salt	2923.33
3310-3350	N-H stretching	secondary amine	3343.01

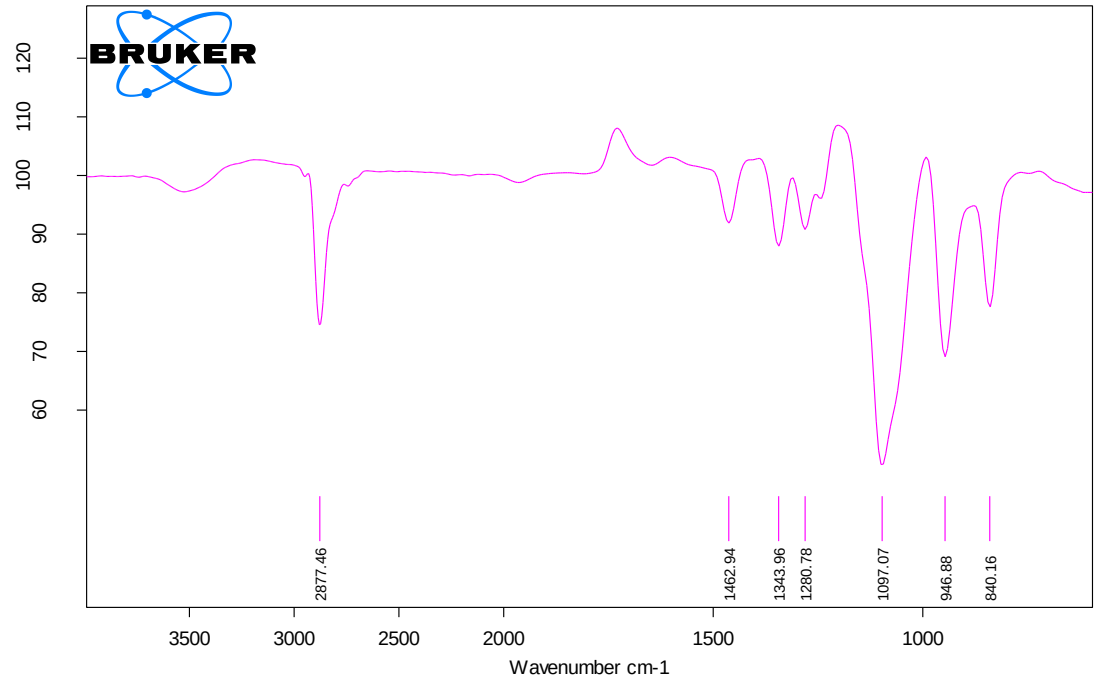

Figure 5 IR of Polyethylene glycol-2000

Table 6 IR interpretation of Polyethylene glycol-2000

Peak Range	Group	Class	Frequencies Determined
790-840	C=C bending	alkene	840.16
1085-1150	C-O stretching	aliphatic ether	1097.07
1250-1310	C-O stretching	aromatic ester	1280.78
1330-1420	O-H bending	alcohol	1343.96
1450-1465	C-H bending	alkane	1462.94
2840-3000	C-H stretching	alkane	2877.46

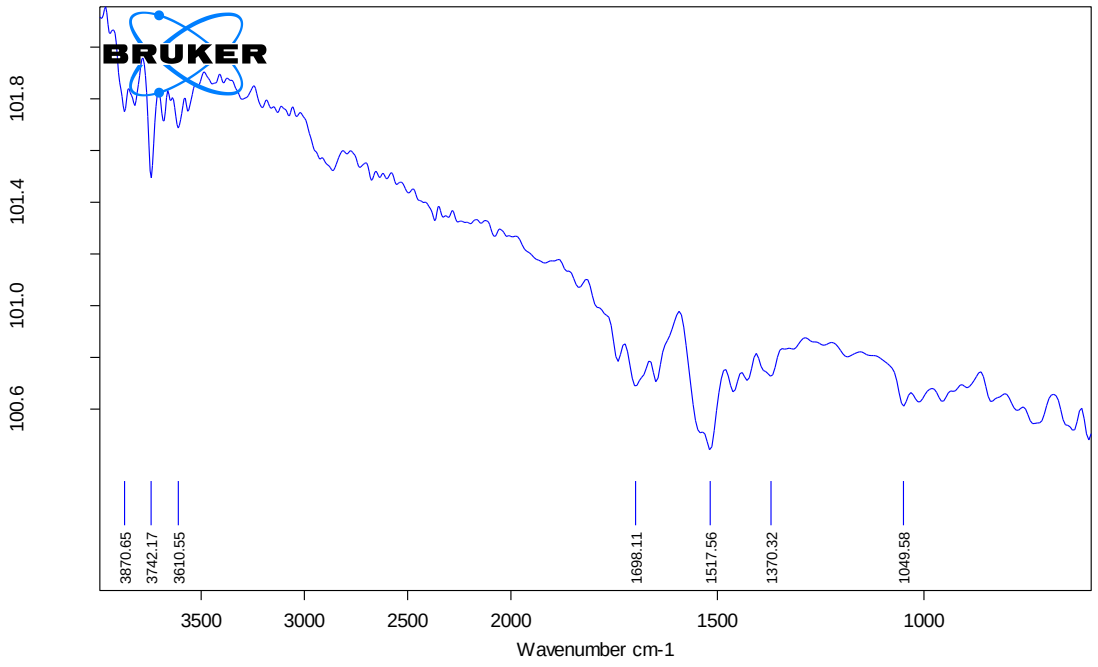

Figure 6 IR of Cholesterol-AR

Table 7 IR interpretation of Cholesterol-AR

Peak Range	Group	Class	Frequencies Determined
1030-1070	S=O stretching	Sulfoxide	1049.58
1335-1370	S=O stretching	sulfonamide	1370.32
1600-1550	N-O stretching	nitro compound	1517.56
1685-1710	C=O stretching	conjugated aldehyde	1698.11

FTIR study of Formulation batches.

Figure 7 IR of Formulation batches F3

Table 8 IR interpretation of Formulation batch F3

Peak Range	Group	Class	Frequencies Determined
3100-3690 cm^-1	Hydroxyl O-H	Alcohols	3563.93 cm^-1
2850-2960 cm^-1	Alkane C-H	Alkanes	2930.39 cm^-1
1700-1750 cm^-1	Ketones and Aldehydes C=O	Carbonyl Compounds	1743.62 cm^-1
1350-1480 cm^-1	Alkanes CH2	Alkanes	1455.18 cm^-1
1000-1300 cm^-1	Ethers C-O	Ethers	1079.84 cm^-1
900-1000 cm^-1	Methyl groups CH3	Alkanes	970.08 cm^-1
700-800 cm^-1	Chlorinated groups C-Cl	Haloalkanes	701.27 cm^-1

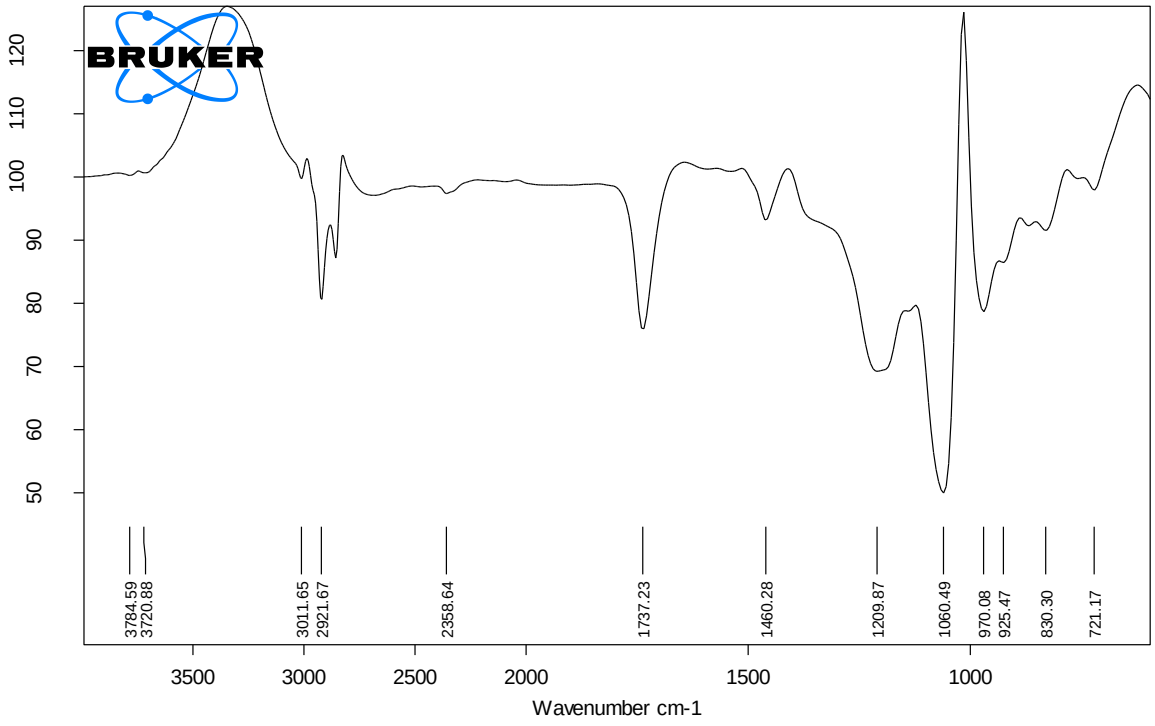

Figure 8 IR of Formulation batches F6

Table 9 IR interpretation of Formulation batch F6

Peak Range	Group	Class	Frequencies Determined
3000-3100 cm^-1	Aromatic compounds C-H	Aromatic hydrocarbons	3011.85 cm^-1
2850-2960 cm^-1	Alkane C-H	Alkanes	2921.67 cm^-1
1700-1750 cm^-1	Ketones and Aldehydes C=O	Ketones/Aldehydes	1737.23 cm^-1
1350-1480 cm^-1	Alkanes CH2	Alkanes	1460.28 cm^-1
1000-1300 cm^-1	Ethers C-O	Ethers	1209.87 cm^-1
900-1000 cm^-1	Methyl groups CH3	Alkyl groups	970.08 cm^-1
700-800 cm^-1	Chlorinated groups C-Cl	Halogenated hydrocarbons	721.17 cm^-1

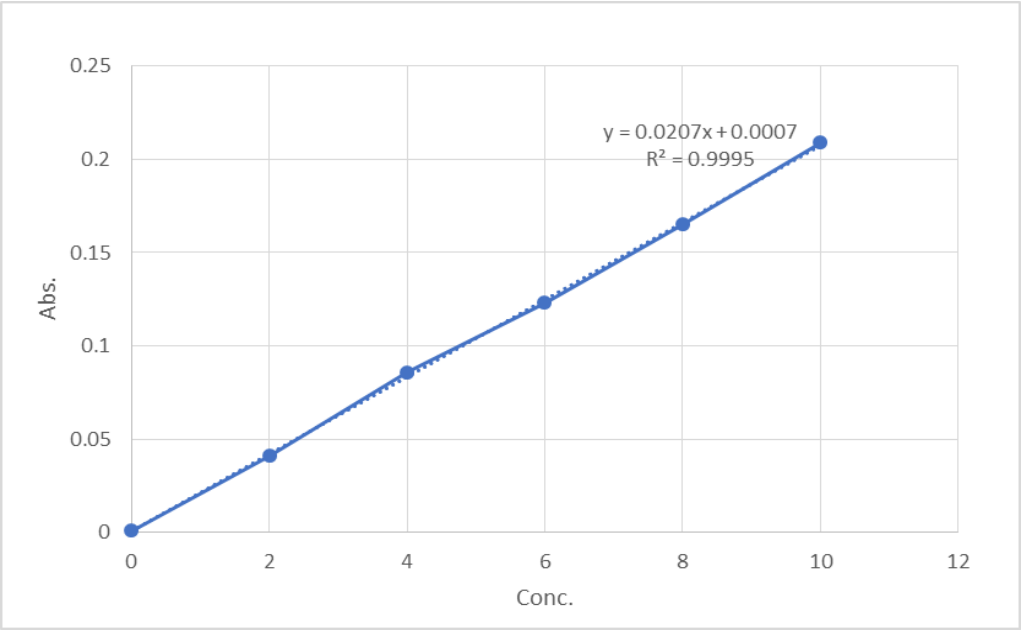

Figure 9 Luliconazole standard curve in DMSO.

Table 10 Absorbance table of Luliconazole standard curve in DMSO.

Sample ID	Ex	Conc.	WL 296	Wgt. Factor
1	Standard	0.000	0.001	1.000
2	Standard	2.000	0.041	1.000
3	Standard	4.000	0.086	1.000
4	Standard	6.000	0.123	1.000
5	Standard	8.000	0.165	1.000
6	Standard	10.000	0.209	1.000

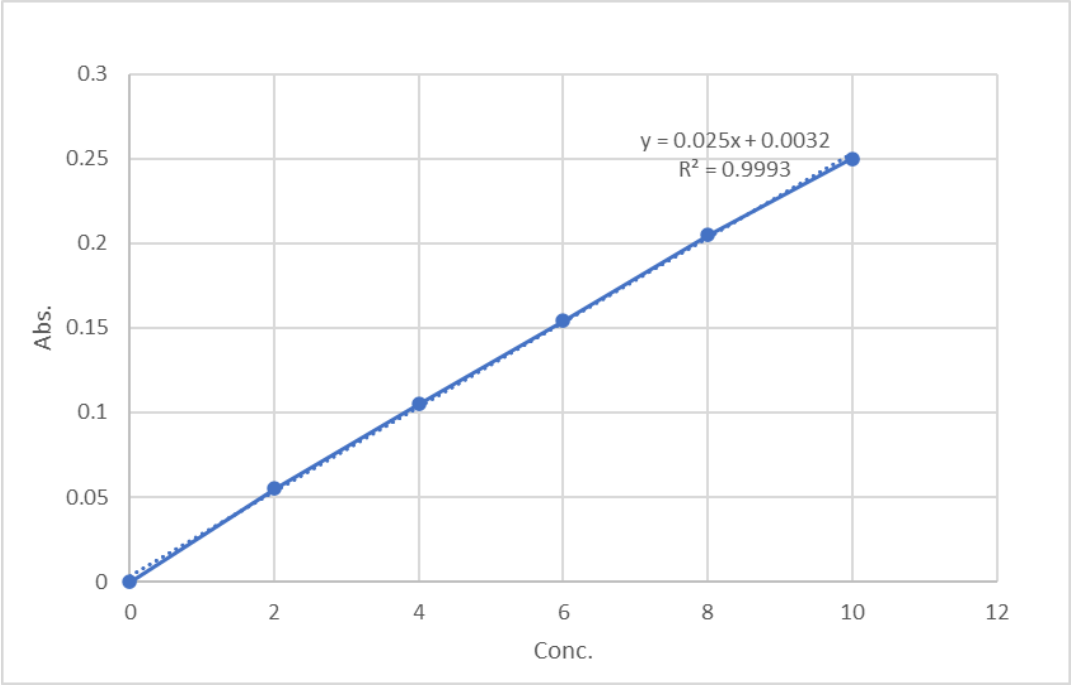

Figure 10 Luliconazole standard curve in Ethanol.

Table 11 Absorbance table of Luliconazole standard curve in ethanol.

Sample ID	Ex	Conc.	WL296	Wgt. Factor
1	Standard	0.000	0.001	1.000
2	Standard	2.000	0.055	1.000
3	Standard	4.000	0.105	1.000
4	Standard	6.000	0.154	1.000
5	Standard	8.000	0.205	1.000
6	Standard	10.000	0.25	1.000

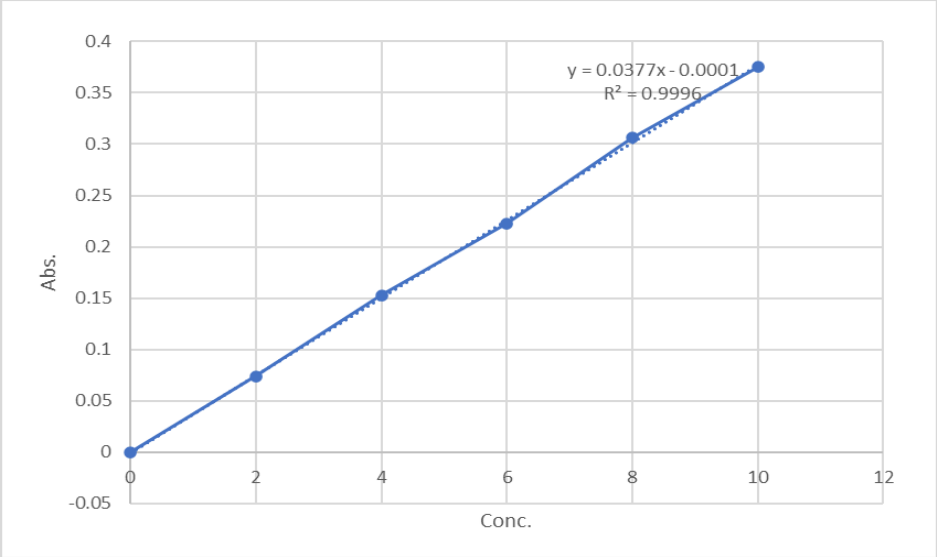

Figure 11 Luliconazole standard curve in phosphate buffer.

Table 12 Absorbance table of Luliconazole standard curve in phosphate buffer.

Sample ID	Ex	Conc.	WL296	Wgt. Factor
1	Standard	0.000	0.001	1.000
2	Standard	2.000	0.074	1.000
3	Standard	4.000	0.153	1.000
4	Standard	6.000	0.223	1.000
5	Standard	8.000	0.306	1.000
6	Standard	10.000	0.375	1.000

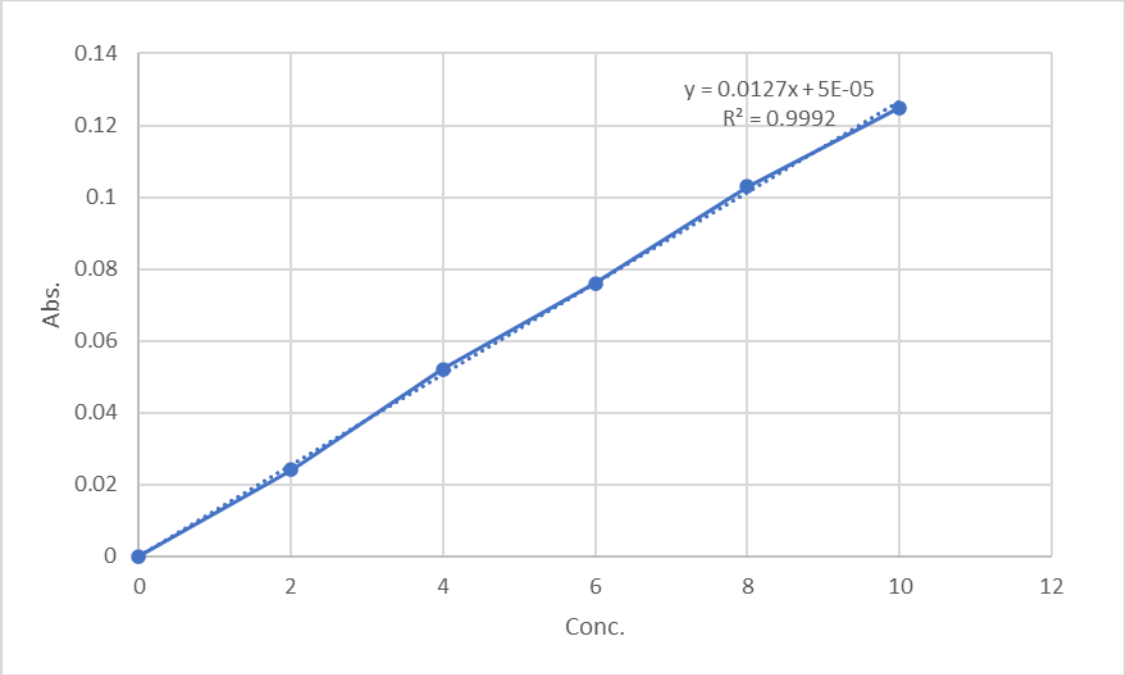

Figure 12 Luliconazole standard curve in water.

Table 13 Absorbance table of Luliconazole standard curve in water.

Sample ID	Ex	Conc.	WL296	Wgt. Factor
1	Standard	0.000	0.001	1.000
2	Standard	2.000	0.024	1.000
3	Standard	4.000	0.052	1.000
4	Standard	6.000	0.076	1.000
5	Standard	8.000	0.103	1.000
6	Standard	10.000	0.125	1.000

Zeta-potential, particle size and Polydispersity index

Particle size and zeta potential are important parameters for understanding colloidal systems. Particle size represents the dimensions of individual particles, while zeta potential measures the electric potential difference at the particle surface. The table of particle sizes and potential is shown below and inclusion of the Polydispersity Index provides information about the particle size distribution within each formulation. A lower PDI value indicates a more uniform particle size distribution, while a higher value suggests a broader range of particle sizes within the formulation.

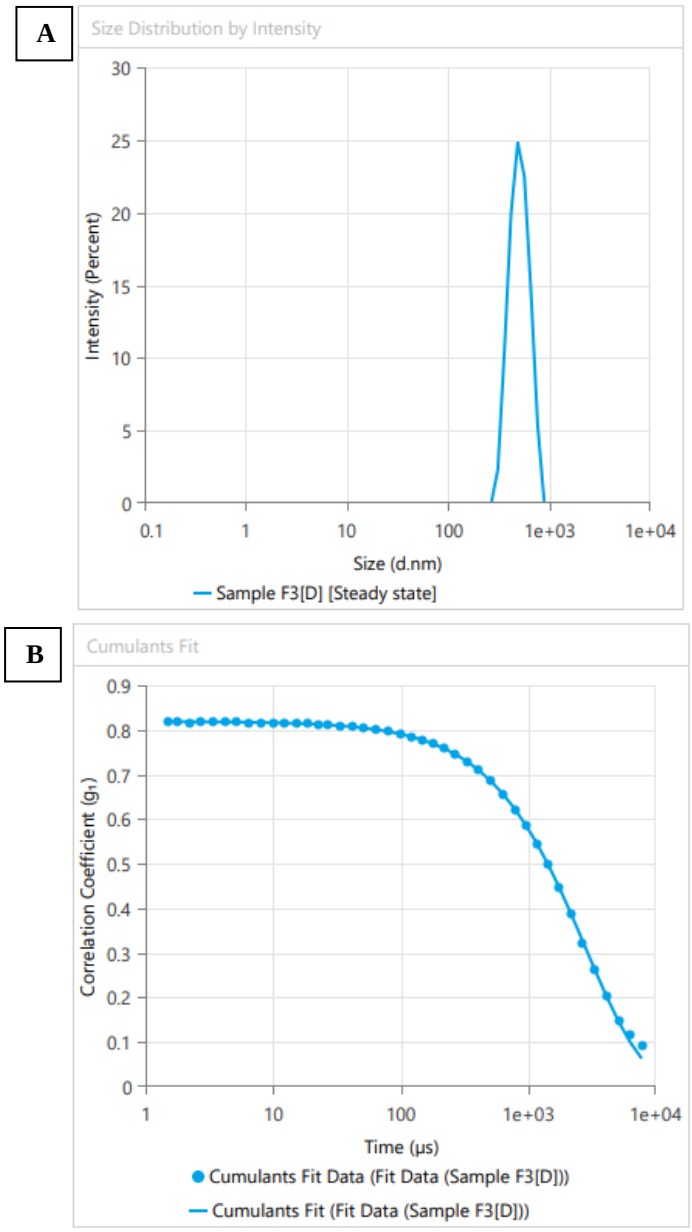

Figure 13: (A) is the size distribution graph wrt intensity and cumulant fit (B) graphical representation of batch F6

Table 14 Average size table of formulation batch F6

Name	Mean	Standard Deviation	RSD	Minimum	Maximum
Z-Average (nm)	302.2	-	-	302.2	302.2
Polydispersity Index (PI)	0.04425	-	-	0.04425	0.04425
Intercept	0.8187	-	-	0.8187	0.8187
Derived Mean Count Rate (kcps)	1569	-	-	1569	1569
Cuvette Position (mm)	4.64	-	-	4.64	4.64
Number Of Size Runs	30	-	-	30	30
Run Retention (%)	95	-	-	95	95
In Range (%)	93.61	-	-	93.61	93.61
Fit Error	0.001142	-	-	0.001142	0.001142
Detector Angle (°)	90	-	-	90	90

4. CONCLUSION

In conclusion, the research on Polymeric Nanoparticles for Optimized Luliconazole Delivery in Tinea Versicolor Management" has systematically addressed the challenges associated with conventional drug delivery systems for treating tinea versicolor. Through the exploration of UV, FTIR, dissolution, zeta sizer and potential, SEM, and optical microscopy techniques, the study has successfully formulated and evaluated polymeric nanoparticles as a promising alternative. The research findings, leading to the synthesis of optimized polymeric nanoparticles. Finally, the results and discussions chapter synthesized the outcomes of characterization and evaluation studies, providing insights into the potential efficacy of the developed nanoparticles in tinea versicolor management. Through this comprehensive exploration, the thesis contributes to the advancement of dermatological therapeutics, offering a promising avenue for improved treatment outcomes in patients with tinea versicolor.

5. REFERENCES

1. Kim, J., Campbell, A. S., de Ávila, B. E. F., & Wang, J. (2019). Wearable biosensors for healthcare monitoring. *Nature biotechnology*, *37*(4), 389-406.
2. Zhang, T., Tang, Y., Guo, S., Cao, X., Pan, A., Fang, G., ... & Liang, S. (2020). Fundamentals and perspectives in developing zinc-ion battery electrolytes: a comprehensive review. *Energy & Environmental Science*, *13*(12), 4625-4665.
3. Liang, S. (2020). Fundamentals and perspectives in developing zinc-ion battery electrolytes: a comprehensive review. *Energy & Environmental Science*, *13*(8), 4724-4765.
4. Yin, L., Cao, M., Kim, K. N., Lin, M., Moon, J. M., Sempionatto, J. R., ... & Wang, J. (2022). A stretchable epidermal sweat sensing platform with an integrated printed battery and electrochromic display. *Nature Electronics*, *5*(10), 694-705.
5. Li, G., Li, C., Li, G., Yu, D., Song, Z., Wang, H., ... & Liu, W. (2022). Development of conductive hydrogels for fabricating flexible strain sensors. *Small*, *18*(5), 2101518.
6. Dong, K., Peng, X., & Wang, Z. L. (2020). Fiber/fabric-based piezoelectric and triboelectric nanogenerators for flexible/stretchable and wearable electronics and artificial intelligence. *Advanced Materials*, *32*(5), 1902549.
7. Lim, H. R., Kim, H. S., Qazi, R., Kwon, Y. T., Jeong, J. W., & Yeo, W. H. (2020). Advanced soft materials, sensor integrations, and applications of wearable flexible hybrid electronics in healthcare, energy, and environment. *Advanced Materials*, *32*(15), 1901924.
8. Qin, J., Yin, L. J., Hao, Y. N., Zhong, S. L., Zhang, D. L., Bi, K., ... & Dang, Z. M. (2021). Flexible and stretchable capacitive sensors with different microstructures. *Advanced Materials*, *33*(34), 2008267.
9. Yang, R., Zhang, W., Tiwari, N., Yan, H., Li, T., & Cheng, H. (2022). Multimodal sensors with decoupled sensing mechanisms. *Advanced Science*, *9*(26), 2202470.
10. Shao, Y., Ying, Y., & Ping, J. (2020). Recent advances in solid-contact ion-selective electrodes: Functional materials, transduction mechanisms, and development trends. *Chemical Society Reviews*, *49*(13), 4405-4465.
11. Kumari, R., Kumar, R., Kumar, S., Singh, A. K., Hanpude, P., Jangir, D., & Maiti, T. K. (2020). Amyloid aggregates of the deubiquitinase OTUB1 are neurotoxic, suggesting that they contribute to the development of Parkinson's disease. *Journal of Biological Chemistry*, *295*(11), 3466-3484.

12. Prajapati, A. K., Sagar, S., & Kumar, R. (2022). Past and Current Prospectives of Herbal Product for Skin Care. *Journal for Research in Applied Sciences and Biotechnology*, *1*(5), 145-160.
13. Butola, K., Bisht, V., & Kumar, R. (2023). Recent Approaches of Ocular Disease and Its Herbal Product Treatment: An Updates. *Journal for Research in Applied Sciences and Biotechnology*, *2*(2), 102-114.
14. Shekhar, S., Kumar, A., Rana, V., Kumar, R., Mittal, C., & Tariyal, K. (2023). Recent Approaches of Matrix Release Tablet in NDDS System. *Journal for Research in Applied Sciences and Biotechnology*, *2*(3), 64-71.
15. Nyarko, R. O., Kumar, R., Sharma, S., Chourasia, A., Roy, A., & Saha, P. (2022). Antibacterial Activity of Herbal Plant-Tinospora Cordifolia And Catharnthus Roseus.
16. Kumar, R., Jangir, D. K., Verma, G., Shekhar, S., Hanpude, P., Kumar, S., ... & Kanti Maiti, T. (2017). S-nitrosylation of UCHL1 induces its structural instability and promotes α-synuclein aggregation. *Scientific reports*, *7*(1), 44558.
17. Havlickova, B., Czaika, V. A., & Friedrich, M. (2008). Epidemiological trends in skin mycoses worldwide. *Mycoses*, *51*, 2-15.
18. Brown, G. D., Denning, D. W., Gow, N. A., Levitz, S. M., Netea, M. G., & White, T. C. (2012). Hidden killers: human fungal infections. *Science translational medicine*, *4*(165), 165rv13-165rv13.
19. Lopes, J. P., & Lionakis, M. S. (2022). Pathogenesis and virulence of Candida albicans. *Virulence*, *13*(1), 89-121.
20. Tang, C., Kong, X., Ahmed, S. A., Thakur, R., Chowdhary, A., Nenoff, P., ... & de Hoog, G. S. (2021). Taxonomy of the Trichophyton mentagrophytes/T. interdigitale species complex harboring the highly virulent, multiresistant genotype T. indotineae. *Mycopathologia*, *186*, 315-326.
21. Lockhart, S. R., Chowdhary, A., & Gold, J. A. (2023). The rapid emergence of antifungal-resistant human-pathogenic fungi. *Nature Reviews Microbiology*, *21*(12), 818-832.